Coexisting phases and lattice dependence of a cellular automaton model for traffic flow

Raissa M. D'Souza*
Microsoft Research, Redmond, Washington 98052, USA
(Received 30 January 2004; published 16 June 2005)

The Biham-Middleton-Levine traffic model is perhaps the simplest system exhibiting phase transitions and self-organization. Moreover, it is an underpinning to extensive modern studies of traffic flow. The general belief is that the system exhibits a sharp phase transition from freely flowing to fully jammed, as a function of initial density of cars. However, we discover intermediate stable phases, where jams and freely flowing traffic coexist. The geometric structure of such phases is highly regular, with bands of free flowing traffic intersecting at jammed wave fronts that propagate smoothly through the space. Instead of a phase transition as a function of density, we see bifurcation points, where intermediate phases begin coexisting with the more conventionally known phases. We show that the regular geometric structure is in part a consequence of the finite size and aspect ratio of the underlying lattice, and that for certain aspect ratios the asymptotic intermediate phase is on a periodic limit cycle (the exact microscopic configuration recurs each τ time steps). Aside from describing these intermediate states, which previously were overlooked, we derive simple equations to describe the geometric constraints, and predict their asymptotic velocities.

DOI: 10.1103/PhysRevE.71.066112 PACS number(s): 89.40.Bb, 64.60.My, 64.60.Cn, 05.20.Dd

I. INTRODUCTION

Modeling vehicular and internet traffic, thereby gaining an understanding of congestion patterns and jamming phenomena, is an extremely relevant problem, with obvious practical ramifications. One popular approach is the use of simple discrete cellular automaton (CA) models, which capture aspects of the dynamics of discrete vehicles or packets. One of the most cited examples of such a CA model is the Biham, Middleton, and Levine model (BML) of two-dimensional traffic flow [1]. At the time of this writing, Ref. [1] has received over 200 citations in the scientific literature, and it serves as a theoretical underpinning for the physicists' approach to modeling traffic. Note that using techniques from physics to model traffic has been a fruitful research area for more than a decade, and continues to be. For recent reviews see Refs. [2–5].

The BML model describes two species of "cars" moving on a two-dimensional square lattice, with periodic boundary conditions. The model is extremely simple, yet the behaviors it displays are extraordinarily complex. The system shows what appears to be a phase transition from having all cars freely moving at all time steps, to complete gridlock, where no car can ever move again. In addition, in all the phases, the system becomes fully correlated, forming a range of interesting stable self-organized patterns. It is perhaps the simplest model where one can study both phase transitions and self organization. This model has recently become increasingly of interest to the combinatorial mathematics community, as it continues to elude rigorous theoretical analysis [6].

We implement the BML model and study its behaviors via computer simulation. We discover stable intermediate states that have never been reported before for the BML model, with highly structured geometric patterns of wave fronts of jams moving through otherwise freely flowing traffic. We show the geometry of these patterns arise due to the finite size and periodic boundary conditions of the underlying lattice. We also show that the aspect ratio of the lattice imposes geometric constraints which restrict the patterns, and derive simple equations describing these geometric constraints which allow us to calculate the asymptotic velocities. For certain aspect ratios we can prove that the intermediate configurations end up on a periodic limit cycle—the exact microscopic configurations recur each τ time steps—hence these states are stable for all time. For the other aspect ratios, we show the intermediate states are at least metastable, lasting as long as we could simulate them. By establishing the existence of these intermediate states, we show that the conventional beliefs about this model need to be reexamined. Contrary to the evidence published elsewhere, only on smaller spaces do we see evidence for a sharp transition from freely flowing to fully jammed configurations as a function of the initial density of cars, ρ. Instead we observe bifurcations as a function of ρ, where different phases can begin to coexist. The bifurcation points, the range of the windows for phase coexistence, and the number of coexisting phases depend on the size and the aspect ratio of the underlying lattice. Considering the amount of ongoing work on this model, and its use in large scale, complex simulations of traffic, we believe it is important to understand these observations.

This article is organized as follows. In Sec. II we review the BML model and relevant past work. In Sec. III we describe our simulations and empirical results. Section IV contains a discussion of the kinetic pathways, geometric constraints, and derivation of the velocities for the intermediate states. Finally, in Sec. V, we summarize and discuss open questions and areas for further inquiry.

II. THE BML MODEL

Consider two species of particles (i.e., "cars"), eastbound and northbound (which we also interchangeably call

*Electronic address: raissa@alum.mit.edu

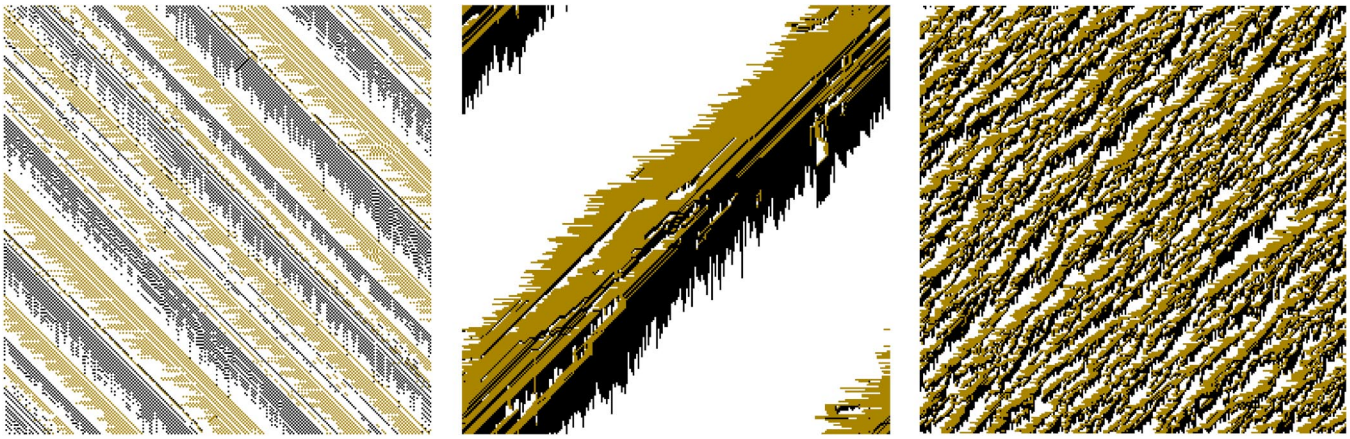

FIG. 1. (Color online) Typical configurations observed for the BML model on an $L \times L$ system of size $L=256$. (a) The free flowing stage, where all particles advance during each update ($v=1$). Note the ordered stripes of alternating east- and northbound cars. The width of the stripes increases, on average, with density ρ while in the low density phase. (b) A fully jammed configuration, consisting of one global jam. Note the jam length $\sqrt{2}L$ is larger than the system size. (c) A high density, random jam configuration.

"brown" and "black," respectively), which populate a two-dimensional square lattice with periodic boundary conditions. Each lattice site can be in one of three states: empty, occupied by an eastbound car, or occupied by a northbound car. The cars are initially distributed uniformly at random along the lattice sites, with spatial density ρ (usually taken to be the same for both north- and eastbound cars). The discrete time dynamics has two phases. On even steps, all eastbound cars synchronously attempt to advance one lattice site toward the east. If the site eastward of a car is currently empty, it advances. Otherwise, it remains stationary (even if the eastward site is to become empty during the current time step). On odd time steps, the northbound cars follow the analogous dynamics, only attempting to advance to the northward site. The dynamics is fully deterministic. The only randomness is in the initial condition. Furthermore, the dynamics conserves cars, and does not allow for an eastbound car to change its row, nor for a northbound car to change its column. So on an $L \times L$ lattice, there are $2L$ conservation laws.

If initialized with a low enough density of cars, the system eventually self-organizes into a configuration where all cars can move at each time step (each car has asymptotic velocity equal to unity). A typical such configuration is shown in Fig. 1(a). If initialized at slightly higher density, the cars are blocked by other cars, until eventually all cars end up participating in one large global jam, where no car can move (asymptotic velocity equal to zero). A typical global jam is shown in Fig. 1(b). The transition between the two behaviors has been thought of as sharp, showing characteristics of a first order phase transition. Initialized at much higher densities, small jams begin simultaneously throughout the lattice and merge almost immediately with other small jams, leaving all cars blocked (with all velocities equal to zero). In this high density phase, the system has no time to self-organize, and instead of one global jam, we observe a collection of small random jams. This latter type of jam has been compared to traffic in a large city during "rush hour:" a car might escape one jam, only to quickly join the tail of the next. We expect that for an infinite size system, the fully jammed state resembles this random type of jam.

Most of the understanding of the BML model has come from numerical simulations [1,7–13]. Theoretical analysis has been limited to mean-field approaches [7,14–16], and attempts to start with continuum hydrodynamic equations and formulate an equivalent discrete model [17]. There are general beliefs about this model, that the transition is first order and that the critical density ρ_c decreases with increasing system size, possibly reaching the value $\rho_c=0$ as the system size approaches infinity [1]. The BML model has been simulated extensively, but there are inconsistencies in the literature and lack of detail of numerical implementations (such as the size of the ensemble being averaged over). Details of numerical studies have been published only for small systems, on the order of $L=10-50$ [7,8]. Larger systems have only been studied coarsely, or in the context of self-organized versus random jams [9,10].

Despite extensive numerical simulation, the existence of stable intermediate phases (with $0<v<1$) has not been explicitly reported previously. Fukui and Ishibashi [8] do show evidence of the existence of an intermediate phase in one plot. They note that for intermediate values of ρ, v "fluctuates around a certain value for a long time." The value shown in their plot is extremely close to the values we observe (plotted in Sec. III). Aside from this comment, they do not pursue the issue further. A careful study by Török and Kertész [11] contains precise details of their numerical simulations. They are studying a variant of BML with faster convergence times (called the green wave model). Since it is not possible to theoretically predict the convergence time, they estimate it, and apply the following, very reasonable, empirical heuristic. If a realization has not reached a state, with $v \approx 0$ or $v \approx 1$, within an allotted time (taken to be five times the estimated convergence time), that realization is discarded. We can only assume some of the studies of the BML model may have used a similar criteria of discarding "non-converged" states. Note that for continuum models, interme-

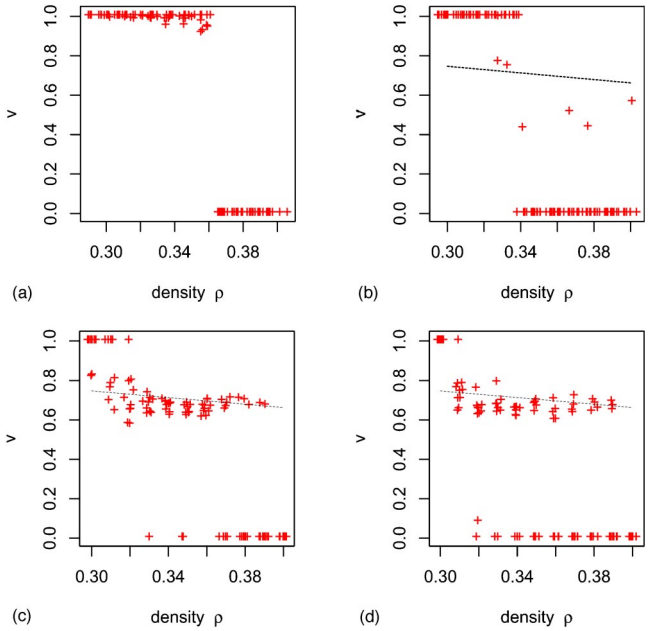

FIG. 2. Plot of the average velocity for each individual realization v versus the density ρ for that realization, for an $L\times L$ lattice: $L=$(a) 64, (b) 128, (c) 256, and (d) 512. Note the emergence of an intermediate phase for $L>64$. The value of v for the intermediate state becomes more crisply defined with increasing system size, and that the window of coexistence between the phases broadens. For the $L=512$ system, the average value of v in the intermediate phase is $\langle v_s\rangle=0.673\pm0.005$. The dotted line shown in (b)–(d) is the prediction from Eq. (24).

diate phases of jammed wave fronts moving through otherwise freely flowing traffic have been reported. See for instance Ref. [18].

Sensitivity of the BML model to boundary conditions has been reported previously. Martínez *et al.* [12] study the dilute limit ($\rho\to0$), and show that different results are obtained for an "entangled" torus versus a conventional one. They raise interesting questions about how to get at the bulk properties using only finite size simulations, but do not quantify nor pursue the effects further. Chau, Wan, and Yan [13] study the BML model on the torus with random boundary conditions (BCs) [meaning that particles moving off the right (top) edge reappear at some randomly selected site on the left (bottom) edge]. They claim $v>0$ whenever $\rho<1$, and hence dismiss such systems as being "not very interesting." They also note that the velocity and critical density depend sensitively on the choice of BCs, but they also do not pursue the effects further.

III. SIMULATION RESULTS

We implement the BML model on square lattices of finite size $L\times L'$, for a range of sizes and varying aspect ratios. For square aspect ratios (i.e., $L=L'$), the lengths studied range from $L=64$ to 512. We also study rectangular aspect ratios where the width L is an integer multiple of the height L', and where L and L' are relatively prime. On each lattice, we implement a range of densities ρ, studying at least ten realizations for each density. All simulations are implemented on a special purpose cellular automata machine, the CAM8 [19]. The CAM8 performs approximately 10^8 site updates per second, comparable to a modern high-performance desktop computer. The main advantage of the CAM8 is that it allows for excellent visualization of the system, with no overhead in the rendering, giving us live video output of the dynamics of the system. As discussed in Sec. IV, visualizing the kinetic pathway gives crucial insight into the formation of the intermediate states.

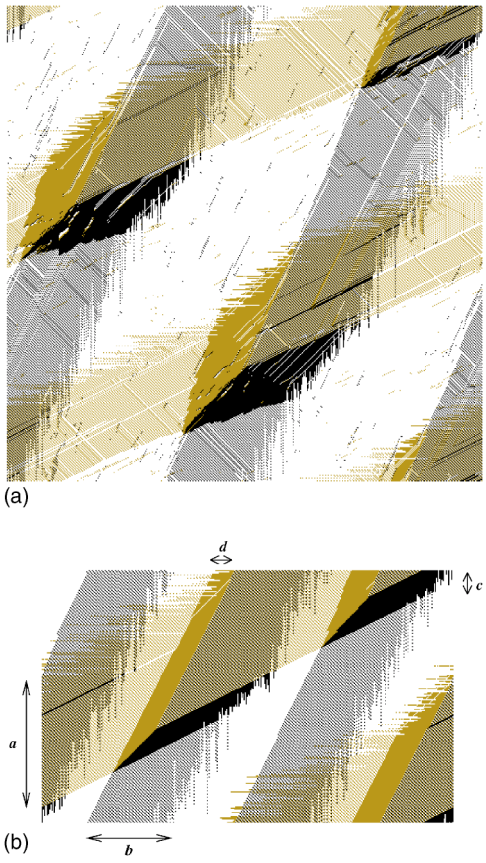

FIG. 3. (Color online) Examples of typical intermediate geometry. (a) A system with square aspect ratio where $L=512$, $\omega_r=1/2$, and $\omega_b=2$, where ω_r and ω_b are winding numbers to be defined in Sec. IV B. (b) A system with rectangular aspect ratio where $L=377$, $L'=233$, $\omega_r=1$, and $\omega_b=3$. Note that in (a) there are many disordered, random cars in the space between the bands, yet in (b) all cars are ordered. We find this crisp order shown by the latter example for all realizations studied on rectangular aspect ratios with L and L' relatively prime. If L and L' are not relatively prime, random disordered cars located between the bands persist. Note that Fig. 9 below is a closeup of the region that has just shed from the jams in (b).

The main subtlety involved with simulating this model is determining the convergence time (i.e., the time it takes to reach the asymptotic behavior). All realizations were simulated until converged ($v=0$, $v=1$, or the periodic limit cycle was reached) or for times out to at least $t=2\times10^6$ time steps. Of the realizations that had not yet converged, many were simulated for orders of magnitude beyond. We find this a reasonable compromise, since the compute power to simu-

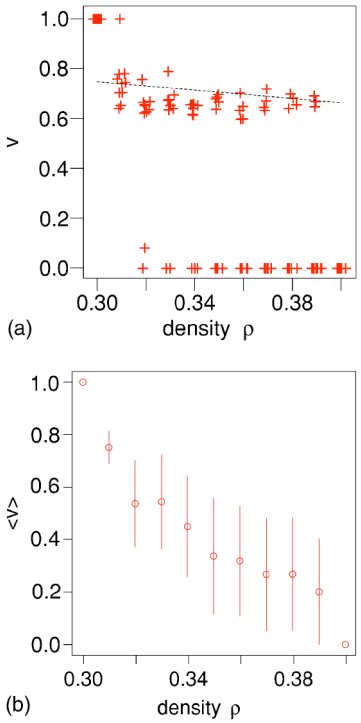

FIG. 4. Comparison of (a) behavior of individual realizations to (b) the behavior of the same realizations averaged together by density, for a square system of $L=512$. Note that by averaging the quantized nature of the final state for each realization is obscured.

late all samples to times greater than 10^8 is beyond our current capacity. Throughout the remainder of the manuscript, we refer interchangeably to the eastbound cars as "brown" and the northbound as "black."

A. Square aspect ratios

For small size systems we actually observe the predicted behavior of a sharp transition from freely flowing to total gridlock. Figure 2(a) is for an $L\times L$ system with $L=64$. It is a plot of the final average velocity observed for each realization v versus the density for that particular realization. Note that we are plotting the average velocity for each individual realization, not an average over all realizations initialized with the same ρ (hence error bars are on the order of the size of the plotting symbol used). Surprisingly, when we implement systems with $L>64$, we observe a bifurcation where two phases start to coexist, as we go from low to intermediate values of ρ. The second phase that emerges has average velocity $v\sim 2/3$, as shown in Fig. 2. In addition, these intermediate states have a very well defined geometry, of bands of brown stripes with slope one-half, criss-crossing bands of black stripes with slope 2. An example of the geometry is shown in Fig. 3. Jammed wave fronts are located at the intersections of the bands, and, as the systems evolves in time, move as solid structures uniformly down toward the southwest with unit velocity. Particles are freed from the head of each jam, but a like number of new jammed particles aggregate at the tail. As discussed in detail below, the underlying lattice imposes constraints on the allowed topologies of the

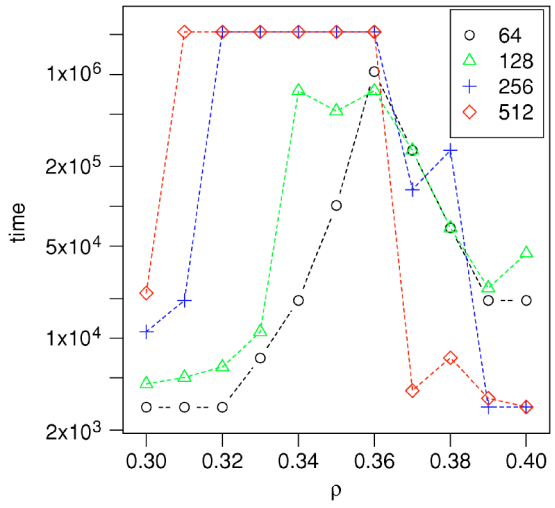

FIG. 5. Median convergence times for the different square system sizes simulated. These results are consistent with previous studies. Note that a value of $t=2\times 10^6$ should be interpreted as $t>2\times 10^6$.

configurations. In Sec. IV, we derive a simple formulation of the constraints.

All realizations contributing to Fig. 2 were simulated to at least $t=2\times 10^6$ full updates of the entire space, with various realizations simulated for $t>10^8$. We do occasionally observe a realization persist in the $v\sim 2/3$ state for orders of magnitude, then suddenly jump to either $v=0$ or $v=1$, with the latter being more common. Regardless, the intermediate state is at least metastable, persisting for longer than we could simulate most realizations. Furthermore it is "universal" in the sense that the value of $v\sim 2/3$ is independent of system size and density, and all systems that do not go to $v=0$ or 1 go to the same intermediate state (i.e., the same geometric structure and approximate value of v). The reason we do not average over the individual realizations is that it would obscure the behavior. Instead of displaying the three distinct quantized states, averaging would produce a deceitfully smoothly decaying curve, as shown for instance in Fig. 4.

From our data, it is difficult to determine the exact bifurcation point where the phases begin to coexist, and the point where they cease to. We attempted to identify the factors that distinguished realizations which converge to $v=0$ from those, with the same density, that converge to $v\sim 2/3$. We first investigated connections to anisotropy, such as an imbalance between the total number of eastbound versus northbound particles. But we found no correlation. The probability a realization would jam or go to the intermediate state is independent of this asymmetry. We also looked at a more fine-grained measure: the line density of brown particles versus the black. Again we found no correlation between this asymmetry and the likelihood of jamming.

In Sec. IV we discuss the kinetic mechanism observed, which gives rise to the interleaved band structure exhibited by the intermediate states. As mentioned above, the jam interface moves ballistically, with unit speed, toward the southwest. The width of the jam interface can fluctuate. It seems

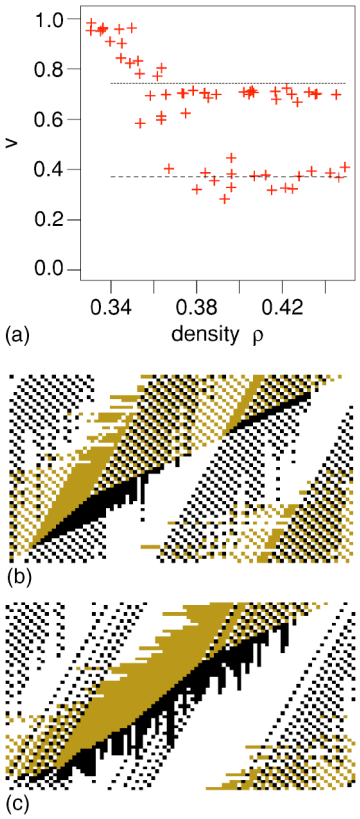

FIG. 6. (Color online) (a) The average velocity for each individual realization v versus the density ρ for that realization, for an $L\times L'$ lattice, with $L=89$ and $L'=55$. Note the appearance of yet another well defined intermediate state. Note also that the bifurcation point, where phase coexistence ceases, has not yet been reached, despite the range of $\rho>0.44$. The dotted lines are the predicted velocities from Eqs. (18) and (21), $v_{r1}\approx 0.7430$ and $v_{r2}\approx 0.3707$. The empirically determined average values are, respectively, $\langle v_{r1}\rangle=0.700\pm 0.002$ and $\langle v_{r2}\rangle=0.364\pm 0.004$. The geometries of the two types of intermediate states are distinct. (b) A typical configuration with $v\sim 2/3$. Interface slope $s=1$. (c) A typical configuration with $v\sim 2/5$. Interface slope $s\approx 2/3$. Note that the interface is the surface where the jammed regions of different colors meet.

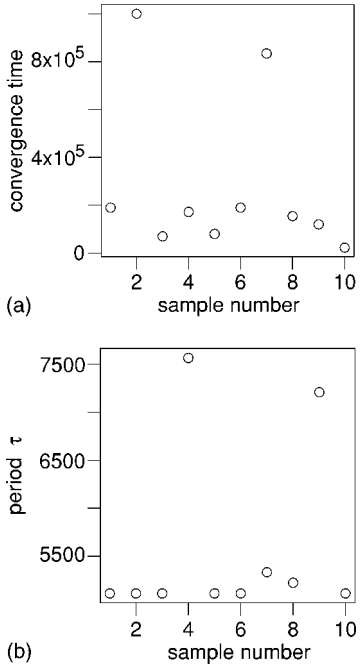

FIG. 7. For simulations with $L=89$ and $L'=55$ and $\rho=0.38$, we plot (a) the time to reach the periodic limit cycle versus sample number; (b) the period of the cycle τ versus sample number. Eight of the ten realizations simulated reach final configurations of type I, as shown in Fig. 6(b). They all have the shorter values of τ. Surprisingly six of these eight realizations have the same period $\tau=5114$, though their microscopic configurations differ. The other two realizations, with significantly larger values of τ, are of type II, as shown in Fig. 6(c).

for the $L=64$ system that the fluctuations are large enough that eventually the head of one jam meets the tail of the previous, continuing until eventually one global jam forms. Figure 5 shows the median convergence times observed for the systems with square aspect ratios. Note that the a value of $t=2\times 10^6$ really means $t>2\times 10^6$.

B. Rectangular aspect ratios

We also implement the BML model on systems with varying rectangular aspect ratios. In particular we study lattices where the two lattice lengths are subsequent Fibonacci numbers. Figure 6(a) is the plot analogous to those shown in Fig. 2, for a system with $L=89$ and $L'=55$. Note we see the same intermediate velocity of $v\sim 2/3$, but we also see the emergence of one more possible phase with $v\sim 2/5$. All the configurations with $v\sim 2/3$ resemble the one shown in Fig. 6(b), with one brown band wrapping around the $\hat{x}$ axis, and three black bands. The jam points are at the intersections of the bands. Note the crisp, regular geometry. Recall Fig. 3(b) which is for an equivalent, but larger, system with the same Fibonnaci aspect ratio but with $L=377$ and $L'=233$. This figure more clearly illustrates the highly ordered geometry. It also includes the definitions of several of the parameters used in the analysis in the subsequent sections. All realizations with $v\sim 2/5$ resemble the one shown in Fig. 6(c), with one brown band and approximately two black bands (though the latter are not so clearly defined).

One of the most striking differences when comparing these rectangular aspect ratios to the square, is that for the rectangular, the intermediate configurations are exactly periodic: the exact microscopic configuration of particles repeats every τ updates. We observe systems of size $L=89$ and $L'=55$, settling into the periodic behavior typically in a time less than $t\sim 100\,000$ updates, with a period on the order of $\tau\sim 6000$ updates. Figure 7 is a plot illustrating such typical behavior. Another striking difference is that not one realization has jammed fully ($v=0$), despite the fact that the largest density simulated is $\rho=0.45$. Note that for the square aspect ratios, the bifurcation point where the phases cease to coexist is at $\rho\approx 0.40$. Another striking differences is the lack of disorder for the relatively prime systems with rectangular aspect ratios. In Fig. 3(a) there are isolated particles ("dislocations")

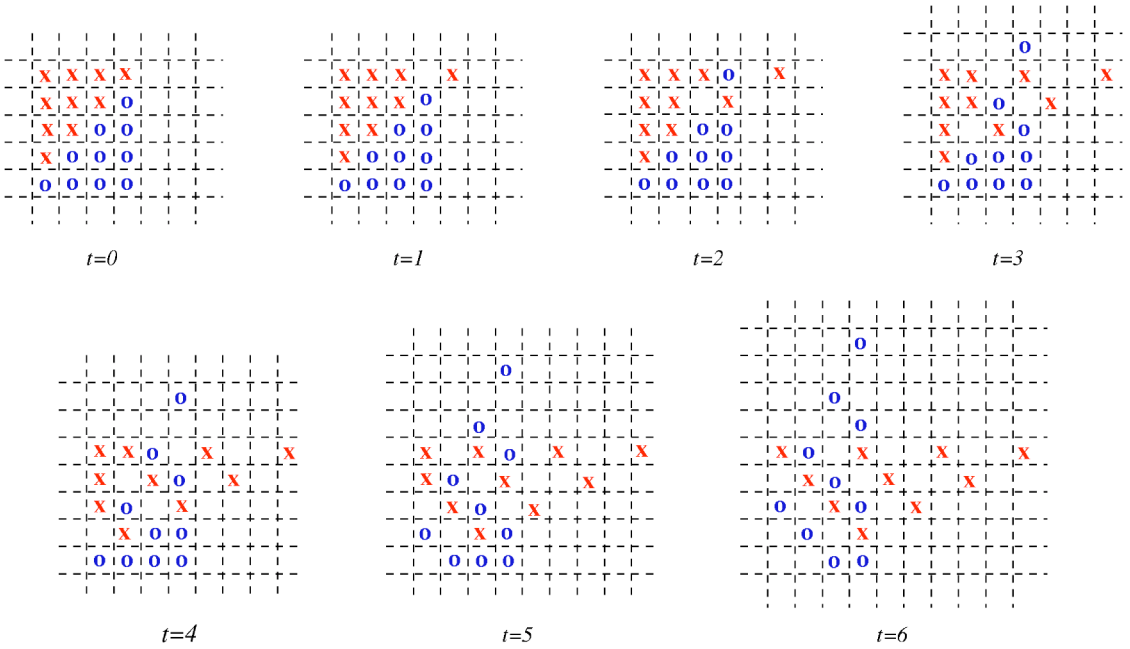

FIG. 8. Shedding from a jam.

moving in the area between the bands. However, for the rectangular case, all the particles manage to join the ordered bands.

IV. GEOMETRIC CONSIDERATIONS

A. Kinetic pathways

By watching the dynamical evolution of the system, starting from the initial configuration, the mechanism by which the intermediate phases form can be observed. Often one global jam initially begins to form, yet the head of the jam just fails to meet up with the tail, leaving a few lattice sites of distance between them. Particles shed from the head as soon as allowed by the local environment (since all particles move whenever possible), leaving with a well defined order. See Ref. [20], for video images of the dynamical evolution.

To understand the pattern formed by the shedding, consider first one row of a solid isolated block of brown particles. Since the particles only advance provided the site they wish to occupy is empty, a particle would leave the head of the jam only every other time step. However, we can now consider a diagonal interface formed by a triangular block of brown particles in contact with a triangular block of black particles. See Fig. 8. Note brown (eastbound) particles are represented by x and black (northbound) particles by o. Each subsequent time step illustrated corresponds to one complete update of the space (i.e., one north step followed by one east step). Recall, all particles of the same species update synchronously. Step 1: No o's are able to move, but, during the east phase of the time step, the first x moves away from the jam, opening up a space. Step 2: The first o advances. This blocks all other x's in the original row, yet opens up a space for an x, one site from the original x along the southwest diagonal, to advance. The original x to move also continues advancing. Step 3: That first o continues advancing and opens up a space for an x in the original row to advance—two time steps delayed from the first x to move in that row. The o below this original o is currently blocked. However, an o one site from the original along the southwest diagonal is now free to advance. Note that this o blocks the x in its newly occupied row from advancing, yet opens up a space for the x one row southward to advance. Hence a pattern emerges: a brown particle sheds from within the same row only every third time step, yet from a site further southwest every time step, yielding brown bands of density $\rho_r = 1/3$ with slope $s_r = 1/2$. Likewise for the black particles, a black particle sheds from within the same column only every third time step, yet from a successive site along the southwest every time step, yielding black bands of density $\rho_b = 1/3$ with slope $s_b = 2$. The jams occur at the intersections of the bands, and the interface of a jam has slope s. Typically, $s = 1$. In Fig. 8 one can see the order beginning to emerge, and the interface with $s = 1$ in the lower left hand corner.

More illuminating is to view a closeup near the jammed regions. Figure 9 is a zoomed-in view of the region near one of the jams shown in Fig. 3(b). Note the order that exists in the region above the jam interface, which has shed from the jam in the manner described above. In this region there are alternating diagonal stripes of black, brown, and empty. The stripes have "phase locked"—on the next update the black stripes move into the empty stripe regions, leaving room for the brown stripes to move on the subsequent update, and so on. Hence the system has organized itself into the highest density packing that still allows all particles to move with $v = 1$.

B. Winding number

Since the system lives on a torus, the bands must wrap seamlessly around it. Noting these facts, we can develop a

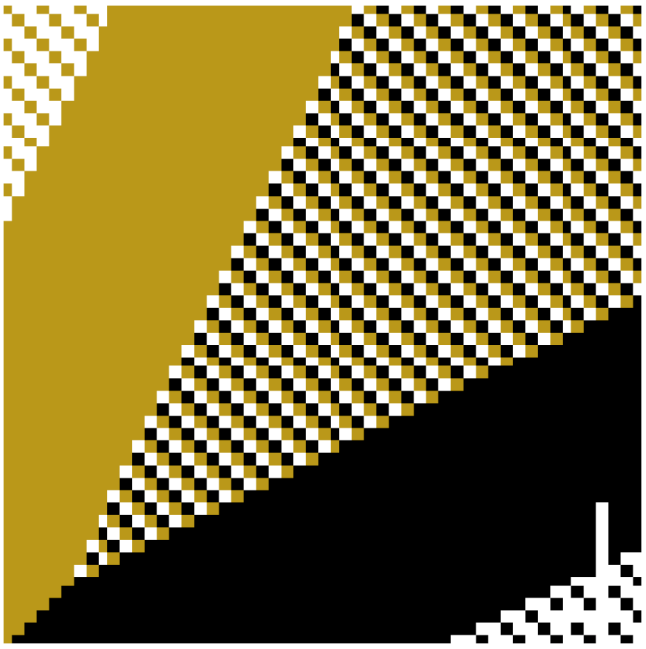

FIG. 9. (Color online) A zoomed in view of a jam shown in Fig. 3(b). The interface of the jam is shown in the lower left hand corner. It is the region where the jams of different colors meet. Note the slope $s=1$.

mathematical expression for the number of brown bands ω_r and the number of black ω_b (referred to, respectively, as the "winding" number for brown and black) that must be present. Essentially, we can calculate the length of the regions of slope $1/2$, slope s, and slope 2 that must be present for the bands to wrap around the torus. (The slopes are respectively those of the brown band, the interface, and the black band.) Consider an $L\times L'$ lattice, and a brown band starting in the lower left hand corner. Moving out along the $\hat{x}$ direction, there are k sites with slope $1/2$ and k' sites with slope s. Similarly for a black band starting in the lower left hand corner, there are m sites with slope 2 and m' sites with slope s. The constraints are

$$k + k' = L, \tag{1}$$

$$\frac{1}{2}k + sk' = \omega_r L', \tag{2}$$

$$m + m' = L, \tag{3}$$

$$2m + sm' = \omega_b L', \tag{4}$$

$$k' = m', \tag{5}$$

where, due to the lattice, $\{k,k',m,m'\}$ are positive integers, and $\{\omega_r,\omega_b\}$ are either positive integers or equal to $1/g$, where g is a positive integer [e.g., for the configuration shown in Fig. 3(a), $\omega_r=1/2$]. The final equation, Eq. (5), expresses that the length of the jam interface must be the same for the brown and black cars. Combining this system (of five equations in seven unknowns), we can solve some

TABLE I. Allowed winding numbers ω_r and ω_b for lattices with different aspect ratios L/L' and interface slope s. The values of v which include error bars are from our numerical simulations.

L/L'	s	ω_r	ω_b	v
1	1	1/2	2	0.673 ± 0.005
1	1	1	1	0
2	1	1	4	$\sim 2/3$
2	1	2	2	0
5/3	1	1	3	$\sim 2/3$
3	1	2	5	$\sim 2/3$
$(1+\sqrt{5})/2$	1.17	1	3	0.700 ± 0.002
$(1+\sqrt{5})/2$	7/10	1	2	0.364 ± 0.004

combination of variables in terms of the others. Solving first for k';

$$k' = (2\omega_r L' - L)/(2s-1). \tag{6}$$

Using this, we can solve for ω_b in terms of ω_r, s, L, and L', and obtain

$$\omega_b = \frac{2L}{L'} - \frac{(2-s)}{(2s-1)}\left(2\omega_r - \frac{L}{L'}\right). \tag{7}$$

Knowing that the interface slope $s\sim 1$, we can tabulate the allowed values of ω_r and ω_b in terms of the aspect ratio of the space, L/L'. The allowed values for various aspect ratios are listed in Table I. Note, the value $\omega_r=1/2$ means the brown band has only reached height $L'/2$ in traversing distance L [as in Fig. 3(a)]. We implement systems with the various aspect ratios shown in Table I, and find that the experimental configurations observed all match the predicted behavior. See in addition to the previous figures, Fig. 10. The final lines in Table I are for systems where we observe empirically the values of ω_r and ω_b, and using Eq. (7) can predict the value of s. Recall that ω_r and ω_b must be integers. The system seems to tune the value of s to allow this. For instance, if L and L' are successive Fibonacci numbers [i.e., $L/L'=(1+\sqrt{5})/2$], a rearrangement of Eq. (7) predicts $s=1.17$, which matches our empirical observations. Note in Fig. 3(b), the upper jam has small glitches where $s>1$.

FIG. 10. (Color online) A typical realization with $L=769$ and $L'=256$ (i.e., $L=3L'+1$, where the additional lattice site is to make the lengths relatively prime). Note that as predicted in Table I, the configuration is consistent with $s=1$, $\omega_r=2$, and $\omega_b=5$. Realizations with $L=768$ and $L'=256$ (i.e., $L=3L'$) have a similar structure, but surprisingly lack the crisp order, and instead have disordered cars at random locations between the bands. For images of the latter, see Ref. [20].

C. Average velocity

Figure 3 illustrates the typical geometry for realizations with $v \sim 2/3$. In this example, $\omega_r = 1$ and $\omega_b = 3$. We label on the figure the lengths a, b, c, and d, denoting, respectively, the width of the brown band, the black band, the black jam, and the brown jam. We define two discontinuous functions which will simplify notation later on:

$$\Theta_r(\omega_r) = \begin{cases} 1 & \text{if } \omega_r \geq 1, \\ 1/\omega_r & \text{if } \omega_r < 1, \end{cases} \tag{8}$$

$$\Theta_b(\omega_b) = \begin{cases} \omega_b & \text{if } \omega_b \geq 1, \\ 1 & \text{if } \omega_b < 1. \end{cases} \tag{9}$$

In other words, Θ_r is the number of independent brown bands in one column of the lattice. Θ_b is the number of independent black bands in one row of the lattice. If we denote the density of the brown band as ρ_a, we can express the average number of brown particles in a column of the space:

$$\Theta_r(\omega_r)\rho_a a = \rho L'/2. \tag{10}$$

Likewise, the average number of black particles in a row is

$$\Theta_b(\omega_b)\rho_b b = \rho L/2. \tag{11}$$

Recall that ρ is the overall particle density (brown plus black). Empirically we determined that $\rho_a = \rho_b = 1/3$, which is a consequence of the dynamics described in Sec. IV A. Using the basic equations described in Sec. IV B and knowledge of the "typical" geometry, we can solve for the velocity of the intermediate state. Unfortunately, we have to consider the square and rectangular aspect ratios independently, and do not have one equation that describes all cases. The assumptions described above are valid for the rectangular aspect ratios, but fail to capture the full behavior of the square ones.

1. Rectangular aspect ratios type I

Configurations such as the one shown in Fig. 3 have a regular, highly structured, geometry that is well described by the formalism in Sec. IV B. We find that the values of k' predicted by Eq. (6) exactly match those obtained via numerical simulation. Typically there are n_j jams, with the particles equally divided amongst them. The interface width per jam is $k_i' = k'/n_k$, where n_k is the total number of jams one brown band is involved in, as it wraps once around the $\hat{x}$ axis. See Fig. 3(a), for example, where $n_k \approx 2$ and $n_j = 3$.

The structure of the jams and the relevant geometric factors are shown in Fig. 11(a). The jams form trapezoidal shapes of width δ. From simple geometric considerations, we can show that $\delta = k_i' \sin(\theta - \phi) \equiv \kappa k_i'$. The jam width per line, d, and per column, c is

$$c = d = \frac{\delta}{\cos \xi} = \frac{\sin(\theta - \phi)}{\cos \xi} k_i' \equiv \Gamma k_i'. \tag{12}$$

However, note this is only true provided that there are enough particles available in each column and in each row. Otherwise,

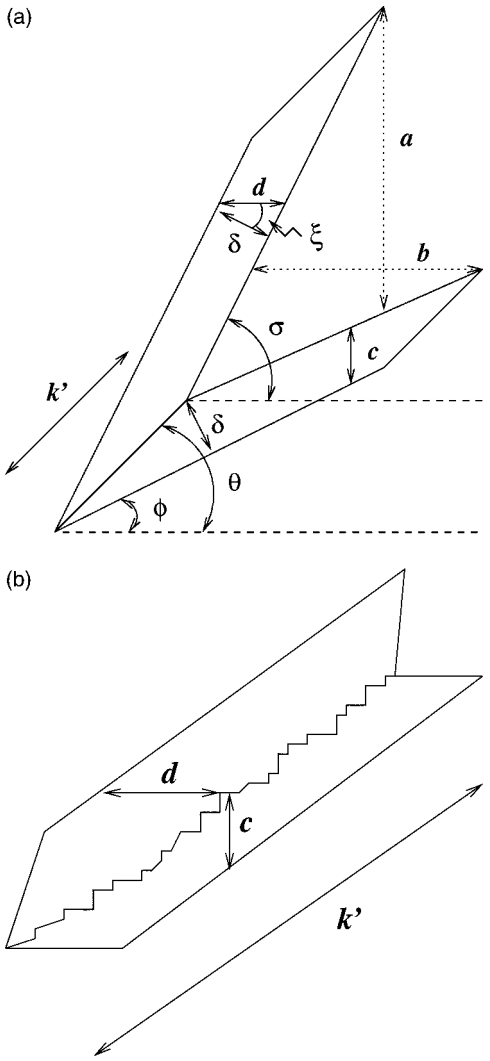

FIG. 11. Typical jam configurations. For type I jams, shown in (a), $c = d = \Gamma k'$. For type II jams, shown in (b), $d = d_{\max}$ and $c = c_{\max}$. Knowing the slopes of the lines in (a), $s = 1$, $s_r = 2$, and $s_b = 1/2$, we can determine all of the angles $\phi = \tan^{-1}(1/2)$, $\theta = \pi/4$, $\sigma = \tan^{-1} 2$, and $\xi = (\pi/2 - \tan^{-1} 2)$.

$$d = d_{\max} = \rho L/2\omega_r \Theta_r(\omega_r) \quad \text{and} \quad c = c_{\max} = \rho L' \Theta_b(\omega_b)/2\omega_b. \tag{13}$$

From similar geometric considerations we can show that the length of the black jam, l_b, is approximately

$$l_b \approx b\left\{\cos \phi + \frac{\sin \phi}{\tan(\sigma - \phi)}\right\} \equiv b\gamma. \tag{14}$$

Similarly, the length of the brown jam, l_r, is approximately

$$l_r \approx a\left\{\cos \xi + \frac{\sin \xi}{\tan(\sigma - \phi)}\right\} \equiv a\varphi. \tag{15}$$

The total number of particles involved in the jams, J, is the number of jams multiplied by the width and length:

$$J \approx n_j \delta(l_b + l_r) = (2\omega_r L' - L)\kappa\left[\left(\frac{3}{2}\rho L/\Theta_b(\omega_b)\right)\gamma + \left(\frac{3}{2}\rho L'/\Theta_r(\omega_r)\right)\varphi\right]\frac{n_j}{n_k}. \quad (16)$$

For the data plotted in Fig. 6, L' and L are two successive Fibonacci numbers, hence $L/L' = (1+\sqrt{5})/2 \equiv \mathcal{F}$. In agreement with expected values shown in Table I, $\omega_r = 1$ [thus $\Theta_r(\omega_r) = 1$] and $\omega_b = 3$ [thus $\Theta_b(\omega_b) = 3$]. For this geometry, $n_j = n_k = 2$. Plugging in these values into Eq. (16),

$$J = (2 - \mathcal{F})\kappa\left[\frac{1}{2}\gamma + \frac{3}{2\mathcal{F}}\varphi\right]\rho LL' \approx 0.2570\rho LL'. \quad (17)$$

Solving for the velocity, noting that the overall number of particles $N = \rho LL'$,

$$v_{r1} = 1 - \frac{J}{N} \approx 0.7430. \quad (18)$$

Note, this is independent of ρ and independent of L and L'. This predicted value for v_{r1} is included in the plot of the experimentally determined velocities, shown in Fig. 6. Note that the calculated value slightly underestimates the number of particles involved in the jam (hence slightly overestimates v_{r1}).

2. Rectangular aspect ratios type II

As mentioned, rectangular lattices are well described by the formalism in Sec. IV. We observe the "rich" jam described above, but also a second type of "depleted" jam (not enough particles). Empirically, all observations of this type have $s \approx 2/3$, and one large jam. See for instance Fig. 6(c). The per row and per column widths of the jams are the maximum, $d_{\max}$ and $c_{\max}$, respectively, since $\Gamma k'$ is greater than the number of particles available in a row or column. A jam interface of length k' and slope s (with $s > 1$) involves k' columns, but only sk' rows. Hence the total number of particles involved in the jams,

$$J = k'(sd_{\max} + c_{\max}) = [(2\omega_r L' - L)/(2s-1)][s\rho L/2\omega_r\Theta_r(\omega_r) + \rho L'\Theta_b(\omega_b)/2\omega_b]. \quad (19)$$

For the realizations contributing to the plot in Fig. 6, $L/L' = (1+\sqrt{5})/2 \equiv \mathcal{F}$, $\omega_r = 1$ [thus $\Theta_r(\omega_r) = 1$], $\omega_b = 2$ [thus $\Theta_b(\omega_b) = 2$], and $s = 2/3$ (which is empirically determined). Plugging these values in we find

$$J = \frac{5}{2}\left(\frac{2}{\mathcal{F}} - 1\right)\left(\frac{7}{20}\mathcal{F} + \frac{1}{2}\right)\rho LL' \approx 0.6293\rho LL'. \quad (20)$$

Thus the average velocity

$$v_{r2} = 1 - \frac{J}{N} \approx 0.3707. \quad (21)$$

We include this predicted value in the plot of Fig. 6. Note the agreement with the experimental data.

3. Square aspect ratios

The typical geometry of an intermediate state for a square lattice is shown in Fig. 3(a). The interfaces and especially the edges of the bands are disordered and jagged. The slope assumptions only hold approximately: $s_r \approx 1/2$ and $s_b \approx 2$. Furthermore, there are several particles moving freely in the low density regions, unlike for the rectangular lattices, where all particles eventually order into the bands and jams. Also unlike for the rectangular lattices [see for instance Fig. 3(b)], the brown and black bands cross through each other without the pronounced shifting upward.

We cannot use the formalism developed above in Sec. IV B for this situation, since that formalism is based solely on geometric constraints of winding seamlessly around the lattice. A configuration on a square lattice with $s_r = 1/2$, $s_b = 2$, $s = 1$, would have $w_r = 1/2$. Plugging into Eq. (6) we find the required length of the overall interface, $k' = 0$. Instead, empirically we find the black jams form a trapezoidal shape of approximate length b and height $a/4$. Likewise the brown jams form a trapezoid of approximate length a and width $b/4$. Each jam has this shape and there are $n_j = 3$ jams altogether (i.e., three distinct intersections of the bands). The number of particles involved in jams, J, is

$$J \approx n_j(ab/4 + ab/4) = 3a^2/2. \quad (22)$$

Using Eq. (10) to solve for a and the fact that the overall number of particles $N = \rho LL'$, we can solve for the fraction of particles in the jammed state:

$$\frac{J}{N} \approx \frac{3}{2}\left(\frac{3}{4}\rho L\right)^2\frac{1}{\rho L^2} = \frac{27}{32}\rho. \quad (23)$$

Hence the velocity

$$v_s \approx 1 - \frac{J}{N} = 1 - \frac{27}{32}\rho. \quad (24)$$

This predicted value v_s is included in the plots of Fig. 2. It captures the features of the experimental data, including the slight decrease in v_s with increasing ρ.

V. DISCUSSION

The BML traffic model is a simple model of a jamming transition with self-organization. In our study, instead of agreement with conventional beliefs, we find stable intermediate configurations with phase coexistence of jammed and free flowing traffic. Such configurations have not been previously reported in the literature, despite the extensive amount of past work on the BML model. Furthermore, these intermediate configurations have interesting geometric and topological properties, with different behaviors resulting as a consequence of different aspect ratios of the underlying lattice. We develop a formalism, based on geometric constraints imposed by the lattice, to predict the asymptotic velocities of the coexisting phases. Visualizing the kinetic pathways of the evolving configurations was a key element in uncovering the existence of the intermediate phases and, moreover, their periodic nature on lattices with relatively prime aspect ratios.

The observations described in this manuscript open up a range of new questions about the BML model.

As mentioned, instead of a phase transition as a function of density, we observe a bifurcation point where the intermediate states first begin appearing, and a second bifurcation point, where they completely cease to appear. Perhaps more interesting than predicting the asymptotic velocities, would be to calculate the locations of the bifurcation points. From our experimental data, the exact location of the bifurcation points are difficult to determine, and moreover, also depend on the aspect ratio of the underlying lattice.

It is possible that there is a sharp phase transition. However, in such a case, the density ρ would not be the appropriate control parameter. Perhaps a more appropriate control parameter would be an interaction energy between northbound and eastbound particles. Note that when in the free flowing state, the north and east particles have moved onto noninteracting lattices. It may be possible that one can define an initial energy based on the overlap or interaction between two lattices, and use that as a control parameter.

A complication which makes theoretical treatment of the BML model difficult is that it is not strictly monotonic. Adding particles to a configuration that is known to jam (i.e., increasing ρ) can actually change the sequence of particle interactions and result in that configuration going to free flowing instead of jamming. Furthermore, it is known that certain discrete models with the same property as BML—namely, that the randomness is in the initial condition, yet the dynamics fully deterministic—can be notoriously difficult to deal with analytically. Examples include bootstrap percolation [21] and the Lorentz lattice gas [22]. We modified the BML model to include a small probability for particles to flip species types at each update. Our preliminary studies, adding this small amount of randomness to the dynamics, suggest that the model with randomness has extremely different geometric properties from the original BML model. In addition, for the model with randomness, we did not observe the intermediate configurations described herein.

ACKNOWLEDGMENTS

This work has benefited greatly from discussions with László Lovász, Alexander Holroyd, and Roman Kotecky.

[1] O. Biham, A. A. Middleton, and D. Levine, Phys. Rev. A **46**, R6124 (1992).
[2] T. Nagatani, Rep. Prog. Phys. **65**, 1331 (2002).
[3] A. Schadschneider, Physica A **313**, 153 (2002).
[4] D. Chowdhury, L. Santen, and A. Schadschneider, Phys. Rep. **329**, 199 (2000).
[5] K. Nagel, Phys. Rev. E **53**, 4655 (1996).
[6] P. Winkler, Y. Peres, E. Friedgut, and L. Lovasz (private communication).
[7] T. Nagatani, J. Phys. Soc. Jpn. **62**, 2656 (1993).
[8] M. Fukui and Y. Ishibashi, J. Phys. Soc. Jpn. **62**, 3841 (1993).
[9] S. Tadaki and M. Kikuchi, Phys. Rev. E **50**, 4564 (1994).
[10] S. Tadaki and M. Kikuchi, J. Phys. Soc. Jpn. **64**, 4504 (1995).
[11] J. Török and J. Kertész, Physica A **231**, 515 (1996).
[12] F. C. Martínez, J. A. Cuesta, J. M. Molera, and R. Brito, Phys. Rev. E **51**, R835 (1995).
[13] H. F. Chau, K. Y. Wan, and K. K. Yan, Physica A **254**, 117 (1998).
[14] Y. Ishibashi and M. Fukui, J. Phys. Soc. Jpn. **63**, 2882 (1994).
[15] J. M. Molera, F. C. Martínez, J. A. Cuesta, and R. Brito, Phys. Rev. E **51**, 175 (1995).
[16] B. H. Wang, Y. F. Woo, and P. M. Hui, J. Phys. A **29**, L31 (1996).
[17] T. Nagatani, Phys. Rev. E **59**, 4857 (1999).
[18] T. S. Komatsu and S. Sasa, Phys. Rev. E **52**, 5574 (1995).
[19] N. H. Margolus, in *Pattern Formation and Lattice-Gas Automata*, edited by A. Lawniczak and R. Kapral (American Mathematical Society, Providence, RI, 1996).
[20] http://research.microsoft.com/users/raissa/bml.htm
[21] A. E. Holroyd, Probab. Theory Relat. Fields **125**, 195 (2003).
[22] G. R. Grimmett, in *Random Walks and Discrete Potential Theory*, edited by M. Picardello and W. Woess (Cambridge University Press, Cambridge, U.K., 1999), pp. 205–213.